HHS Public Access

Author manuscript

J Mech Behav Biomed Mater. Author manuscript; available in PMC 2021 November 01.

Published in final edited form as:

J Mech Behav Biomed Mater. 2020 November ; 111: 103945. doi:10.1016/j.jmbbm.2020.103945.

Enhanced osteogenesis of 3D printed β-TCP scaffolds with *Cissus Quadrangularis* extract-loaded polydopamine coatings

Samuel F. Robertson, **Susmita Bose***

W. M. Keck Biomedical Materials Research Laboratory, School of Mechanical and Materials Engineering, Washington State University, Pullman, WA, 99164-2920, USA

Abstract

Growing demand in bone tissue replacement has shifted treatment strategy from pursuing traditional autogenous and allogeneic grafts to tissue replacement with bioactive biomaterials. Constructs that exhibit the ability to support the bone structure while encouraging tissue regeneration, integration, and replacement represent the future of bone tissue engineering. The present study aimed to understand the osteogenic and mechanical effects of binder jet 3D printed, porous β-tricalcium phosphate scaffolds modified with a natural polymer/drug coating of polydopamine and *Cissus Quadrangularis* extract. Compression testing was used to determine the effect the polydopamine coating process had on the mechanical strength of the scaffolds. 3D printed scaffolds with and without polydopamine coatings fractured at 3.88 ± 0.51 MPa and 3.84 ± 1 MPa, respectively, suggesting no detrimental effect on strength due to the coating process. The osteogenic potential of the extract-loaded coating was tested *in vitro,* under static and dynamic flow conditions, and *in vivo* in a rat distal femur model. Static osteoblast cultures indicated polydopamine-coated samples with and without the extract exhibited greater proliferation after 3 days ($p < 0.05$). Similarly, polydopamine resulted in increased proliferation and alkaline phosphatase expression under dynamic flow, but alkaline phosphatase expression was significantly enhanced ($p < 0.05$) only in samples treated with the extract. Histological analysis of implanted scaffolds showed substantially more new bone growth throughout the implant pores at 4 weeks post-op in polydopamine and extract-loaded implants compared to pure β-tricalcium phosphate. These results indicated that implants coated with polydopamine and *Cissus Quadrangularis* extract facilitated osteoblast proliferation and alkaline phosphatase production and improved early bone formation and ingrowth while maintaining mechanical strength.

*Corresponding author. sbose@wsu.edu (S. Bose).

Credit author statement

Sam Robertson: Methodology, Data Curation, Formal Analysis, Writing-Original Draft, and Editing. **Susmita Bose:** Conceptualization, Supervision, Writing-Review and Editing.

Declaration of competing interest

The authors declare that they have no known competing financial interests or personal relationships that could have appeared to influence the work reported in this paper.

Appendix A. Supplementary data

Supplementary data to this article can be found online at https://doi.org/10.1016/j.jmbbm.2020.103945.

Keywords

3D printed scaffolds; Osseointegration; Osteogenic properties; Dynamic cell culture; Bioreactor; Direct drug delivery

1. Introduction

Synthetic bone replacement scaffolds are desired alternatives to autogenous and allogeneic bone grafts, for their potential to preclude a secondary harvest surgery and graft rejection. Understandably, material selection for the scaffold is a critical aspect as the scaffold supports the defect site while facilitating osteogenesis and the regeneration of native bone. Some of the most promising candidates for replacement are calcium phosphate (CaP) ceramics, which chemically resemble the inorganic portion of bone. β-tricalcium phosphate (β-TCP, $Ca_3(PO_4)_2$) is one such CaP that has garnered much attention in the field as it offers the advantages of being biocompatible, bioactive, and biodegradable. In order to more closely resemble the hierarchical structure of natural bone, particularly the cancellous regions, 3D printed scaffolds with designed porosity have been utilized (Bose et al., 2017; Marques et al., 2017). Particularly, scaffolds with pores ranging from 200 to 400 μm have shown increased biocompatibility by allowing greater cell penetration, revascularization, and osseointegration (Vu and Bose, 2019; Karageorgiou and Kaplan, 2005). Despite this, achieving large pore diameters can result in a trade-off between biocompatibility and mechanical strength. β-TCP scaffolds manufactured with random porosity exhibited higher compressive stregnths over scaffolds engineered with 350 μm pore diameters. Yet, the random pores ranged in diameter from 50 to 300 μm, and osteoblast cultures indicated better proliferation on the scaffolds engineered with 350 μm pores (Vu and Bose, 2020).

To increase the bioactivity of CaP scaffolds, bioactive molecules such as growth factors or drugs have been explored as options for direct drug delivery (Ishack et al., 2017; Tarafder and Bose, 2014). Despite their potential, synthetic drugs can carry side effects, driving the need for naturally derived compounds that are better tolerated over sustained use and can be metabolized by the body (Bose and Sarkar, 2020). The plant *Cissus Quadrangularis* or "Hadjod," meaning "bone-setter," has long been used in Ayurvedic medicine as a salve or herbal supplement to treat patients with bone fractures and help offset low bone mineral density. Traditionally, a poultice containing Hadjod was placed around the fracture site or powdered plant was ingested to prevent osteoporosis, while current interest has focused on extractions of the plant (Siddiqua and Mittapally, 2017; Stohs and Ray, 2013). *Cissus Quadrangularis* extract (CQE) is commercially characterized by ketosteroid content via methanolic extraction and gravimetric analysis. Three ketosteroids of interest: β-sitosterol, α-amryone, and friedelin are believed to affect the estrogen signaling pathway. Due to their structural similarity to estrogen, they present a possible method to inhibit bone resorption (Aswar et al., 2010). CQE has been used previously *in vivo* through oral administration and intramuscular injections with little research on *in vitro* cultures. Of these, ethanolic extractions of CQE has shown increased runt-related transcription factor-2 (Runx2) expression and matrix mineralization in cultures of human osteoblast-like cells *in vitro* (Muthusami et al., 2011) and increased alkaline phosphatase (ALP) and mineralization in

mouse osteoblasts (Parisuthiman et al., 2009). When these extractions were orally administered to ovariectomized rats, researchers measured an increase in bone density and breaking strength, and concluded there could be anti-osteoporotic effects of CQE similar to estrogen (Aswar et al., 2012). When studies compared CQE to the selective estrogen receptor modulator, Raloxifene, CQE was found to decrease tartrate-resistant acid phosphatase (TRAP) levels. This indicated a decrease in osteoclast activity, and was backed by enhanced bone tissue restoration in histological analyses (Potu et al., 2009; Shirwaikar et al., 2003). Additionally, CQE has been shown to have anti-inflammatory properties, down-regulating inflammation-stimulating mediators such as cyclooxygenase COX and 5-lipoxygenase 5-LOX (Bhujade et al., 2012). These effects may help CQE play a roll in mitigating inflammation, and expedite recovery in the early healing process.

In order to deliver drugs from bone scaffolds in a controlled manner, polymers are often used. The natural polymer polydopamine (PD) contains both catechol and amine groups that make it a versatile binder (Lee et al., 2007). This adhesive property makes PD a useful biomimetic surface modifier and biomolecule immobilizer (Ku et al., 2010; Lee et al., 2009). A solution containing 2 mg/mL of dopamine hydrochloride (dopamine HCl) has been described as a biomimetic approach to coat a variety of substrates (Lee et al., 2007), and such coatings formed on poly(l-lactide) and polycaprolactone scaffolds resulted in increased extracellular matrix formation and osteogenesis (Lee et al., 2016; Rim et al., 2012). In addition, polydopamine has not only been shown to assist in hydroxyapatite (HA) crystallization (Kim and Park, 2010; Ryu et al., 2010;), but has also been recently used to coat different calcium phosphate polymorphs for biomaterial applications (Forte et al., 2018; Kao et al., 2018; Wang et al., 2019). These coatings showed increased surface wettability (Forte et al., 2018; Wang et al., 2019) and stem cell proliferation and differentiation (Kao et al., 2018; Wang et al., 2019). As a natural binder, biocompatible PD coatings may be used to modify drug release from β-TCP scaffolds while acting as favorable surfaces for protein and cell adhesion, and cell proliferation.

It is difficult to determine the effects that bone tissue engineering scaffolds will have on bone healing using traditional *in vitro* methods. Conversely, *in vivo* is not always viable and smaller sample sizes can be limiting. Therefore, it is essential that *in vitro* studies mimic *in vivo* conditions as closely as possible. To this end, using bioreactors to pump cell media across substrates can more closely simulate the conditions that cells experience *in vivo. Dynamic flow* is crucial to facilitating nutrient delivery and waste removal as well as simulating oxygen tension, substrate strain, and shear stress (Bancroft et al., 2002). It has been previously shown that fluid flow rates play a more significant role in cellular mechanotransduction leading to differentiation and osteogenesis than mechanical loading or strain (Li et al., 2009; Zhao et al., 2018). As such, perfusion flow rates for porous scaffolds have been examined between 0.1 and 10 mL/min (Jagodzinski et al., 2008; Vetsch et al., 2017) with rates between 0.1 and 1 mL/min exhibiting the greatest osteogenic potential (Gaspar et al., 2012). Mesenchymal stem cells cultured on scaffolds have shown perfusion is the dominant stimulus for proliferation, and therefore maximizing perfusion should be the focus of implants (Vetsch et al., 2017). Additionally, bone cells cultured in dynamic conditions exhibit different morphologies and gene expression compared to the same type of cells under static conditions.

In this study, the effects of PD coatings on CQE release and the mechanical strength of the β-TCP scaffolds are examined. This study also investigated the effects of the coating and drug on the osteogenic potential of 3D printed scaffolds *in vitro* and *in vivo*. Compression testing was used to understand how the PD coating process affects the scaffold strength with respect to cancellous bone. Additionally, a release study was conducted in order to understand the effects of PD coating parameters on CQE release under normal and inflammatory conditions. Furthermore, *in vitro* and *in vivo* studies were performed with human fetal osteoblasts under static and dynamic flow conditions and within a rat distal femur model. The effects of the PD + CQE on proliferation and osteogenic potential of osteoblasts was assessed with MTT and ALP assays, while histology was used to evaluate osteogenesis and osseointegration.

2. Methods and materials

2.1. Substrate preparation

In this experiment, β-TCP powder was synthesized by solid-state synthesis using calcium carbonate (CaCO3, Millipore Sigma, ≥ 99.0%) and calcium phosphate dibasic (CaHPO4, Millipore Sigma, 98.0–105.0%) mixed together at a molar ratio of 2:1. The mixture was ball-milled for 12 h at a 2:1 powder to ball ratio and calcined at 1050 °C. After calcining, the powder was mixed with ethanol at 1.5 mL/g for 6 h at a 2:1 ball to powder weight ratio. The powder was dried and washed repeatedly with deionized water over a Buchner funnel and filter paper (Whatman, grade 1) to remove inorganic salts present in the powder. The powder was dried and sieved below 43 μm prior to loading into a binder jet 3D printer (ExOne Innovent^{+}®, Pittsburgh, PA). Scaffolds were printed using methods described in previous research (Tarafder et al., 2013a), and the parameters are described in Supplementary Table S1. Briefly, scaffolds were printed with a designed pore size of 400 μm and cured after printing at 175 °C for 1.5 h, depowdered, and sintered at 1250 °C. Final pore size and porosity measurements were included in Supplementary Table S2. All samples were autoclaved prior to cell culture. For ion and drug release, β-TCP powder was pressed into 12 × 2.5 mm disks at 145 MPa using a uniaxial press and sintered at 1250 °C.

2.2. Polydopamine coating

PD coatings were produced by submersion of the substrates in a buffered dopamine solution. Dopamine HCl [β-(3,4-dihydroxyphenyl)-ethylamine hydrochloride 98%), Millipore Sigma] was weighed out and dissolved in 0.05 M Tris-buffered solution adjusted to a pH of 8.5. To compare the effects of different coating parameters, starting solutions of 0, 2, 5, and 10 mg/mL dopamine HCl concentration were prepared and separated into 4-dram vials at 5 mL aliquots. Pure β-TCP will be referred to as TCP, while coating treatments will be referred to as TCP + PD2, 5, or 10. For ion and drug release profiles, a disk was added to each vial and placed in a shaker at 37 °C for 24 h. *In vitro* and *in vivo* scaffolds were biomimetically coated using filter-sterilized (0.22 μm, Falcon) solutions of 2 mg/mL dopamine HCl as described in the literature while shaken at 37 °C for 24 h (Lee et al., 2007). All samples were washed three times in DI water to remove unattached or excess PD and unreacted dopamine before oven drying at 60 °C. Supplementary SEM images show the substrate surfaces prior to drug loading (Fig. S1.).

2.3. Cissus Quadrangularis Extraction and loading

Commercially available *Cissus Quadrangularis* Extract (Jiaherb, 15% w/ w ketosteroids) was used as the ketosteroid source for this experiment. Methanol was used to separate the ketosteroids from the commercial powder by first solubilizing the commercial powder at 60 °C then filtering the solution through a vacuum-assisted Buchner filter and filter paper (Whatman, grade 1). The ketosteroid extract collected will be referred to as CQE for the remainder of the paper. After drying at room temperature, the extract was solubilized in methanol at 5 mg/mL and passed through a sterile filter (0.22 μm, Falcon) before use in cell cultures. To examine cytotoxicity on osteoblasts, CQE was aliquoted into cell media at 0, 1, 10, 25, 50, 100, and 200 μg/mL concentrations. Drug-loaded scaffolds for *in vitro* and *in vivo* studies were first coated with PD2, then loaded with CQE by dropwise addition until 200 μg or 500 μg loading was reached. These compositions are referred to as CQEL and CQEH, respectively.

2.4. Ion and drug release

Ion and CQE release measurements from PD coated disks were carried out by submerging each composition (TCP, TCP + PD2, PD5, PD10) in 0.1 M phosphate buffer (PBS, pH 7.4) and acetate buffer solutions (ABS, pH 5). For drug release, 1 mg of CQE was added to samples from each composition by dropwise addition. Triplicates of drug-loaded and blank samples not loaded with CQE were submerged in 4 mL of each solution and placed under constant shaking at 37 °C. Solutions for drug release were collected at 2 h, 4 h, 6 h, 12 h, 24 h, and every third day with fresh buffer replaced at each time point. Collected buffers were spun down at 2500 × *g* to ensure debris removal prior to measuring absorbance via UV–Vis spectroscopy microplate reader (BioTek Synergy 2 SLFPTAD, BioTek) at 276 nm. The absorbance values for each set of blanks (TCP, TCP + PD2, PD5, PD10) were used as baselines for the respective CQE-loaded samples. Solutions for ion release were collected every day for the first week, every other day for the second week, and twice a week thereafter and replenished with fresh buffer each time. Calcium ion concentration was measured using inductively-coupled plasma-mass spectroscopy (Agilent, model 7700 ICP-MS).

2.5. Compression testing

Samples for compression testing were made similarly to *in vivo* scaffolds in the binder jet printer. Briefly, 10.7 × ø 7 mm cylindrical scaffolds with 400 μm designed porosity. The scaffolds were cured at 175 °C for 1.5 h, then depowdered and sintered at 1250 °C. Some samples were then taken to be coated with PD prior to compression testing (Shimadzu, Japan). The specimens were compression loaded until failure at a crosshead speed of 0.03 mm/min.

2.6. Cell culture

2.6.1. Seeding—Prior to the start of all cell cultures, all scaffolds were sterilized by autoclaving at 121 °C for 50 min. TCP + PD2 and CQE_L/CQE_H compositions were coated in sterile conditions as described in sections 2.2 and 2.3. Human fetal osteoblast cells (hFOB, ATCC) were used for these cultures and Dulbecco's Modified Eagle Medium

(DMEM) with 10% v/v fetal bovine serum was used as growth medium. The cells were kept in an incubator at 34 °C under an atmosphere of 5% CO_2, and the media changed every 3rd day. The initial cytotoxicity test for CQE was conducted using CQE-loaded DMEM at concentrations described in section 2.3. Cells were seeded directly onto the wells of 96-well plates at 5,000 cells/cm^2 with 6 wells assigned to each CQE concentration. After 3 and 5 days of culture proliferation was analyzed using MTT analysis. The Static culture scaffolds were kept in 24-well plates and cells were seeded directly onto the scaffolds at a density of 4 × 10^4 cells/ scaffold. 1 mL of DMEM was added to each well and cells were cultured until 3, 7, and 11-day time points. Dynamic culture samples were similarly seeded, and given a 24 h period of static culture for cells to adhere. This was referred to as “day 0,” and samples were then transferred into the reactor chambers as shown in (Fig. 1(c)). The media was perfused using a peristaltic pump at 1 mL/min flow rates, and the 200 mL media reservoirs were changed on day 5. Samples were collected for SEM, MTT, and ALP on days 5 and 10.

2.6.2. Cell morphology—Cell morphology was assessed for day 3, 7, and 11 of static culture as well as days 5 and 10 for the dynamic culture. Scaffolds were fixed in 2% glutaraldehyde 2% paraformaldehyde in 0.1 M phosphate buffer at 4 °C for 24 h then post-fixed with osmium tetroxide before dehydration by a graded alcohol series. The samples were gold-coated and imaged by a field-emission scanning electron microscope (FESEM).

2.6.3. Proliferation assay—Osteoblast cell viability was evaluated using MTT (3-(4,5-dimethylthiazol-2-yl)-2,5-diphenyl tetrazolium bromide) assay. MTT solution was prepared by dissolving 5 mg of MTT (Millipore Sigma, St. Louis, MO) per 1 ml of sterile-filtered PBS. Cell media was removed and replaced by 900 µl of fresh media followed by the addition of 100 µl of MTT solution, and the samples were incubated for 2 h. MTT solubilizer was prepared using 10% Triton X-100, 0.1N HCl, and isopropanol. After incubation, 1 mL of solubilizer was added to dissolve the formazan crystals. 100 µl of the final solution was transferred into a 96-well plate in triplicate and read by UV–Vis spectroscopy microplate reader at 570 nm.

2.6.4. Osteogenesis assay—Osteogenesis was evaluated by measuring the production of ALP, an indicator of osteoblast maturation and mineralization capacity of the osteoblast cells. The relative production of the ALP enzyme was quantified following the instructions in the colorimetric ALP kit (SensoLyte® *p*NPP Alkaline Phosphatase Assay Kit, AnaSpec, Fremont, CA). Briefly, samples were washed in the provided buffer solution, then scraped off of the samples into fresh buffer solution supplemented with Triton X-100 at a 1:500 v/v ratio. The cells and buffer were incubated at 4 °C in microcentrifuge tubes for 10 min, then centrifuged at 2500 × g for 10 min. 50 µL of supernatant from each sample was added to a 96-well plate in triplicate. 50 µL of *p*NPP was added to each well, incubated at room temperature for 45 min before being measured with the UV-VIS spectroscopy microplate reader at 405 nm.

2.7. Rat in vivo model

In vivo surgeries were carried out with 6, 12-week-old male Sprague-Dawley rats (Envigo) using a rat distal femur model as previously described (Vu et al., 2019). Surgeries performed

on the animals were in accordance with the protocol approved by the Washington State University Institutional Animal Care and Use Committee (IACUC). In brief, prior to surgery, the rats were given buprenorphine at 0.03 mg/kg, shortly afterward they were induced with isoflurane at 4–5% concentration and maintained at 1–3%. The hind legs were sheared and cleaned with 70% isopropyl and chlorhexidine before an iodine scrub and the animal placed in a sterile field. From the lateral side, an incision was made 1 cm above the knee, cutting between the fascia to reach the lateral epicondyle. Bicortical defects were made with diamond drill bits starting at 1 mm in diameter and increasing by increments of 0.5–3 mm. The site was lavaged with sterile saline to remove bone particles and prevent overheating. The implant was placed snugly into the defect, the fascia sutured together, and the wound stapled closed. This was repeated for the opposite femur. Scaffold compositions of TCP, TCP + PD2, and CQEL were chosen randomly, so that each animal had two different compositions, and the total number of implants per composition was n = 4 for the study. At the end of 4 weeks, the animals were euthanized, and the femur harvested and placed into formalin for histology. Histology was performed by embedding the femurs in Spurr resin, sectioned using a diamond saw, and ground to thin slices. A Masson Goldner Trichrome stain was used to stain old bone, osteoid, and nuclei.

2.8. Statistical analysis

The data for ion and drug release, compressive strength, and the MTT and ALP assays is presented as mean ± standard deviation. Statistical analysis was performed on the compressive strength of pure and polydopamine-coated samples (n = 6) and the MTT and ALP assays (n = 3) using single-factor ANOVA followed by pairwise comparison of the means using Tukey's Method. A p-value < 0.05 was considered significant.

3. Results

3.1. Ion release

Ion release was first measured to determine if PD coatings would hinder or facilitate degradation of TCP in both physiological PBS buffer (pH 7.4) as well as an acidic acetate buffer (pH 5) used to simulate the acidic conditions experienced at wounds under inflammatory conditions. Release profiles showed that at pH 7.4, there was an inverse relationship between the number of calcium ions present in solution and the amount of dopamine HCl used to coat the samples. As the dopamine HCl concentration used for coating increased, the cumulative calcium ion release over 4 weeks decreased. This result was not seen in the pH 5 buffer, where all samples released similar amounts of calcium ions. High standard deviation in 5 mg/mL samples precluded its use over 10 mg/ mL concentrations for further study (See Fig. 2).

3.2. Compression testing

Compression tests were carried out on 400-micron designed pore scaffolds with and without PD coatings. The results (Fig. 3) showed both TCP and TCP + PD2 samples exhibited compressive strengths of ~3.8 MPa, and an average Young's Modulus of ~327 MPa was calculated from stress-strain curves (not shown). No statistical difference in strength or modulus was seen between the two treatments.

3.3. Cell culture and drug release

MTT optical density values (Fig. 4(a)) showed no cytotoxicity between the ranges of 1 and 50 μg at either time point. It should be noted that the lower concentrations of CQE, 1 and 10 μg, showed higher viability than control on day 5. Drug release profiles of CQE on TCP + PD samples (Fig. 4(b)) were collected from a physiological PBS buffer (pH 7.4) as well as in an acetate buffer (pH 5), which was used to simulate the acidic environment created during an inflammatory response. It was observed that higher concentrations of dopamine HCl used to coat the samples resulted in a greater release of CQE into both buffer solutions. Additionally, polydopamine-coated samples kept in acidic buffers showed notably higher release of the drug compared to samples in pH 7.4 that were similarly coated. CQE release was increased by 7.6% and 21.7% in acidic conditions compared to physiological pH for PD2 and PD10 compositions, respectively.

SEM imaging of osteoblasts cultured on scaffolds under static media flow conditions (Fig. 5) showed cells initially attaching to all compositions with no discernable difference in cellular morphology on day 3. On day 7, morphologies were similar, however on samples with loaded with CQE, more precipitate formation could be seen in pockets within the scaffolds that harbored cells. By day 11, cells on TCP samples appeared broader with smooth features compared to the treatment compositions. Cells on all treatment samples appeared more integrated into the scaffold surface and pores.

The static culture MTT assay (Fig. 6(a)) indicated slow initial proliferation across all compositions on day 3, with CQE_L and CQE_H compositions showing significantly higher optical density values than the control. By day 11, cell proliferation had increased, but no statistical difference could be found between the treatment and control samples. Results from the ALP assay (Fig. 6(b)) showed that while relative ALP expression was increasing, there was no difference between control and treatments.

SEM imaging of osteoblasts cultured on scaffolds under dynamic flow conditions (Fig. 7) showed cells initially attaching to all compositions on day 0 with pure TCP samples showing slightly more elongated morphologies. At this time point, crystal formations can be seen on all of the samples. Cell morphologies at day 5 and 10 timepoints appear more flattened and well-integrated into the surface of the scaffolds for all compositions. These crystals can only be seen on the CQE-loaded samples on day 5, and all compositions lack the flake-like crystal formations seen at earlier time points.

Under dynamic culture conditions, the TCP + PD2 scaffolds loaded with 200 μg CQE had a significant effect on osteoblast proliferation by day 10 (Fig. 8(a)). While no statistically relevant difference was seen on day 5, it was noted that MTT mean optical density increased from the addition of PD2 and of PD2 + CQE_L. The osteogenic potential of the cells was also increased, as seen by the day 10 ALP results (Fig. 8(b)), which showed significantly greater ALP expression in CQE_L samples over pure TCP.

3.4. In vivo rat model

Histological results (Fig. 9) showed bone growing to and along the surface of the implants without any indication of fibrosis. While the bone grew to the surface of the β-TCP

scaffolds, there was little bone growth within the pores. TCP + PD2 implants showed bone growing along the inner surfaces of the scaffolds as well as through the centers of the pores. The most bone ingrowth was seen with CQE_L compositions, where a significant amount of mineralized bone was found around the outside of the implant, as well as along the walls and throughout the entire channel of the pores.

4. Discussion

One of the critical aspects of β-TCP use in bone tissue engineering is its ability to be resorbed by the body. Therefore, one of the first aspects of this study was to measure the effect of initial dopamine HCl concentrations on the dissolution of β-TCP in pH 7.4 and pH 5 to mimic physiological conditions as well as acidic conditions caused by an inflammatory response due to injury. Over 4 weeks, it was shown that there was an inverse relationship between the initial amount of dopamine HCl used to coat the samples and the calcium ion concentration in the buffer solutions. The release of calcium ions from β-TCP disks in PBS solution (Fig. 2(a)) was highest in samples that were not coated in PD. For the first week, ion release correlated to the amount of dopamine HCl used to coat samples, after which ion release from PD2 and PD5 were indistinguishable, while PD10 had the lowest ion release over the month. Calcium ion release in acetate buffer (Fig. 2(b)) was nearly identical for all compositions with very little standard deviation. Polydopamine has been shown to facilitate apatite formation in physiological pH (Forte et al., 2018; Kim and Park, 2010), and resulted in more precipitation than β-TCP controls, as seen in the *in vitro* SEM images. As the amount of dopamine HCl used for coating increased, more PD aggregation was seen on the substrate surfaces (Fig. S1.). Increased availability of hydroxyl groups from the catechol units in PD (Fig. 1(b)), which were not involved in surface adhesion, can facilitate calcium precipitation (Ryu et al., 2010). The binding of free calcium ions with the negatively charged hydroxyl groups could explain the decrease in calcium ion release in pH 7.4 in coatings formed using higher dopamine HCl concentrations. Conversely, in pH 6 or lower, the reprecipitation kinetics of CaPs is thermodynamically unfavorable (Lu and Leng, 2005) and explains why no discernable difference in ion release is seen between coated compositions and β-TCP.

The compressive strength of the scaffolds (Fig. 3) measured ~3.8 MPa, which was within the physiological strengths of cancellous bone ranging 2–17 MPa (Morgan and Keaveny, 2001), and were in good agreement with cancellous bone strength in the distal femur (Chunjuan Du et al., 2006). Although the strength of the scaffolds were within physiological limits, it has been shown that higher strengths can be obtained by changing the substrate chemistry via dopants (Tarafder et al., 2013b). Optimizing printing parameters and pore design are also critical steps to achieving higher strengths by increasing solids loading and decreasing porosity between particles. Moreover, additional post-processing such as polymer infiltration can also increase toughness and fracture strength (Baino et al., 2019). Submerging the samples in PD is a non-line-of-site process that can coat the internal surfaces of the scaffolds, but is known for producing nanometer-thin films. The compression testing showed no detrimental effects caused by soaking scaffolds in the PD solution nor beneficial effects on the strength and modulus caused by the coating. Maintenance of the mechanical

properties provided a basis from which drug release and osteogenic potential of PD and CQE could be tested.

In order to validate the use of the methanolic extract of CQE in direct drug delivery, cytotoxicity of varying concentrations of the drug in media was tested. MTT results showed that on day 3, only concentrations of 100 and 200 μg/mL of CQE significantly decreased the optical density below that of the control wells, as shown in Fig. 4(a). On day 5, MTT results showed an increase in optical density for the negative control, 1, and 10 μg/mL concentrations above the control mean. The trend from the 3 and 5-day time points suggests the addition of CQE from 1 μg/mL up to 50 μg/mL did not have deleterious effects, with a trend of greater proliferation up to 10 μg/mL concentrations. This is in good agreement with previous *in vitro* studies with ethanolic extracts of CQE (Muthusami et al., 2011; Parisuthiman et al., 2009). From this, it was concluded that up to 50 μg/mL release was tolerated by the cells, with higher viability seen between 1 and 10 μg/mL over time.

Furthermore, to determine how PD would affect CQE release from TCP substrates, a release study was conducted in the buffer solutions used for the dissolution study. In general, hydrophilic drugs loaded onto substrates without any surface modification will exhibit burst release behavior, where most or all of the drug is released into the aqueous media within 24 h. Whereas with hydrophobic drugs, there is little to no release without hydrophilization or excipients like lysosomes to carry the drug into aqueous media (Kalepu and Nekkanti, 2015; Sarkar and Bose, 2019). PD chains are known to interact through parallel stacking of the indole-dopamine units (Liebscher, 2019; Liebscher et al., 2013). The lack of reactive groups on the ketosteroids present in CQE suggests CQE and PD may interact similarly through noncovalent interactions like charge sharing or hydrogen bonding. Additionally, in higher pH conditions, the catechol units are deprotonated and charge sharing between CQE and PD may reduce release. As pH drops, the catechol units become protonated and can disrupt charge sharing and hydrogen bonding. The isoelectric point of PD is 4, and the weaker overall charge on PD may help explain increased elution of CQE from the substrates in the acidic buffer (Liebscher, 2019).

Release results (Fig. 4(b)) showed there was no burst release seen in physiological pH and only a small percentage of the drug was eluted in total. In contrast, the release profiles revealed a correlation between the amount of dopamine HCl used in the coating reaction and increased elution in acidic conditions. Control TCP loaded with CQE showed negligible differences in total release between acidic or physiological pHs. This demonstrated that CQE was not made any more soluble in acidic conditions. Yet, PD2 and PD10 samples showed both greater initial and long-term release at pH 5, releasing 21.6 % and at 36.9 % of the total loaded CQE over 4 weeks, respectively. In contrast to this, the total amount of CQE released in pH 7.4 was 12.5, 14, and 15% for TCP, PD2, and PD10, respectively. The burst release behavior in acidic conditions can be beneficial as CQE and the ketosteroids it contains have shown possible anti-inflammatory properties (Bhujade et al., 2012), and mitigating the initial inflammatory response can be beneficial in accelerating the healing process (Yu et al., 2016).

Following the cytotoxicity and drug release data, 200 and 500 μg were chosen as low and high CQE loading amounts on PD2 coatings for *in vitro* studies, respectively. On day 3, MTT optical density values (Fig. 6 (a)) showed that both CQE_L and CQE_H compositions were significantly greater than pure TCP. This was not seen on days 7 or 11, although the mean values were greater than control at the end of the study. The ALP assay (Fig. 6(b)) showed no difference between the treatments at 7 and 11 days, indicating the effect of PD or CQE on osteoblasts may have been negligible. The MTT results from the dynamic flow culture (Fig. 8(a)) showed that the perfusion flow regimen resulted in higher baseline optical density values for all compositions compared to static flow. This aside, except for day 3 MTT, no difference could be seen between the static culture compositions; however, in the dynamic setting, the same compositions showed a significant increase in CQE_L samples on day 10. Moreover, significantly higher ALP expression was also observed from osteoblasts on CQE_L scaffolds on day 10 in the dynamic culture (Fig. 8 (b)). The enhanced baseline MTT and ALP values in the dynamic culture are indicative of increased proliferation caused by perfusion flow. The discrepancy between the compositions within the two cultures was thought to be the result of a mitigated initial burst release caused by the transfer of samples to the reactor chambers after the 24 h incubation period. The media flow could have also assisted in drug elution throughout the study. When examining sample surface morphology, differences between TCP, TCP + PD2, and CQE_L compositions could be seen in both static (Fig. 5) and dynamic (Fig. 7) cultures. TCP samples all time points for both studies showed no signs of apatite crystal formation, whereas both TCP + PD2 and CQE_L samples showed crystallite formation at the early time points. Interestingly, precipitate crystals that were present at earlier time points were not observed on any samples on day 10. This suggested the reprecipitation of calcium ions released by the scaffolds was prevented by media flow, and the crystals formed during the 24 h static period "day 0" were dissolved.

The most substantial evidence for the effect of PD and CQE on osteogenesis lies in the 4-week *in vivo* study (Fig. 9). This showed that after 4 weeks, bone had grown to some of the pure TCP scaffold surfaces, but with little or no penetration throughout the pores. In contrast, TCP + PD2 and CQE_L scaffolds showed newly formed bone throughout the pores, and the bone tissue had grown not only along the surface of the implants but in the open space between the scaffold struts as well. These findings indicated the PD2 coating alone was effective in enhancing osteogenesis. Furthermore, the combination of PD2 coating and CQEL loading showed the best performance in terms of increased osteoconductivity and osteogenesis within 4 weeks, a relatively short time for bone healing to occur to this degree. This showed that dynamic *in vitro* cultures better correlated with the *in vivo* results, indicating both PD2 and CQE_L had postive effects on osteogeneis through osteoblast stimulation. Previous work also demonstrated possible estrogenic behavior with CQE in oral dosing (Aswar et al., 2012, 2010; Potu et al., 2009; Shirwaikar et al., 2003). Further study of this coating and drug with mesenchymal stem cells as well as osteoclasts is needed to understand osteoinductive effects, and possible anti-osteoporotic properties.

5. Conclusions

The results of this work demonstrated that the addition of PD coatings increased total CQE release from TCP by 2.6 % at pH 7.4 and 24.4 % at pH 5, providing an avenue for increased

drug release at the early stages of bone healing where acidic environments occur. Additionally culturing osteoblasts in dynamic conditions lead to higher MTT and ALP values compared to static cultures for each respective treatment. Furthermore under the flow regimen described here, CQE_L scaffolds showed a significant increase in cell proliferation and ALP expression. Moreover *in vivo* results showed that the CQE_L scaffolds greatly enhanced osteogenesis and bone ingrowth within the 3D structures compared to β-TCP controls. This study indicated that PD was an effective surface modifier for CQE release, especially in acidic conditions, and that modification of TCP with PD + CQE_L had a significant effect on bone cells and new bone development. In conclusion the use of PD and CQE on bone tissue engineering scaffolds for direct drug delivery can enhance early time point bone healing.

Supplementary Material

Refer to Web version on PubMed Central for supplementary material.

Acknowledgments

The authors would like to thank the financial support from the National Institute of Arthritis and Musculoskeletal and Skin Diseases (NIAMS-R01-AR-066361), as well as acknowledge the Franceschi Microscopy and Imaging Center at Washington State University for their assistance and use of imaging equipment. Mr. Robertson would also like to thank Indranath Mitra and Naboneeta Sarkar for acquiring images, and Yongdeok Jo for his help with mechanical testing.

References

Aswar UM, Bhaskaran S, Mohan V, Bodhankar SubhashL., 2010. Estrogenic activity of friedelin rich fraction (IND-HE) separated from Cissus quadrangularis and its effect on female sexual function. Pharmacogn. Res. 2, 138–145. 10.4103/0974-8490.65507.

Aswar UM, Mohan V, Bodhankar SL, 2012. Antiosteoporotic activity of phytoestrogen-rich fraction separated from ethanol extract of aerial parts of Cissus quadrangularis in ovariectomized rats. Indian J. Pharmacol. 44, 345–350. 10.4103/0253-7613.96310. [PubMed: 22701244]

Baino F, Fiume E, Barberi J, Kargozar S, Marchi J, Massera J, Verné E, 2019. Processing methods for making porous bioactive glass-based scaffolds—a state-of-the-art review. Int. J. Appl. Ceram. Technol. 16, 1762–1796. 10.1111/ijac.13195.

Bancroft GN, Sikavitsas VI, Dolder J, Sheffield TL, Ambrose CG, Jansen JA, Mikos AG, 2002. Fluid flow increases mineralized matrix deposition in 3D perfusion culture of marrow stromal osteoblasts in a dose-dependent manner. Proc. Natl. Acad. Sci. Unit. States Am. 99, 12600–12605. 10.1073/pnas.202296599.

Bhujade AM, Talmale S, Kumar N, Gupta G, Reddanna P, Das SK, Patil MB, 2012. Evaluation of Cissus quadrangularis extracts as an inhibitor of COX, 5-LOX, and proinflammatory mediators. J. Ethnopharmacol. 141, 989–996. 10.1016/j.jep.2012.03.044. [PubMed: 22484053]

Bose S, Sarkar N, 2020. Natural Medicinal Compounds in Bone Tissue Engineering. Trends in Biotechnology 38 (4), 404–417. 10.1016/j.tibtech.2019.11.005. [PubMed: 31882304]

Bose S, Tarafder S, Bandyopadhyay A, 2017. Effect of chemistry on osteogenesis and angiogenesis towards bone tissue engineering using 3D printed scaffolds. Ann. Biomed. Eng. 45, 261–272. 10.1007/s10439-016-1646-y. [PubMed: 27287311]

Du Chunjuan, Ma Hongshun, Ruo Min, Zhang Zhongjun, Yu Xiaojun, Zeng Yanjun, 2006. An experimental study on the biomechanical properties of the cancellous bones of distal femur. Bio Med. Mater. Eng. 16, 215–222.

Forte L, Torricelli P, Bonvicini F, Boanini E, Gentilomi GA, Lusvardi G, Bella ED, Fini M, Nepita EV, Bigi A, 2018. Biomimetic fabrication of antibacterial calcium phosphates mediated by

polydopamine. J. Inorg. Biochem. 178, 43–53. 10.1016/j.jinorgbio.2017.10.004. [PubMed: 29049953]

Gaspar DA, Gomide V, Monteiro FJ, 2012. The role of perfusion bioreactors in bone tissue engineering. Biomatter 2, 167–175. 10.4161/biom.22170. [PubMed: 23507883]

Ishack S, Mediero A, Wilder T, Ricci JL, Cronstein BN, 2017. Bone regeneration in critical bone defects using three-dimensionally printed β-tricalcium phosphate/ hydroxyapatite scaffolds is enhanced by coating scaffolds with either dipyridamole or BMP-2. J. Biomed. Mater. Res. B Appl. Biomater. 105, 366–375. 10.1002/jbm.b.33561. [PubMed: 26513656]

Jagodzinski M, Breitbart A, Wehmeier M, Hesse E, Haasper C, Krettek C, Zeichen J, Hankemeier S, 2008. Influence of perfusion and cyclic compression on proliferation and differentiation of bone marrow stromal cells in 3-dimensional culture. J. Biomech. 41, 1885–1891. 10.1016/j.jbiomech.2008.04.001. [PubMed: 18495131]

Kalepu S, Nekkanti V, 2015. Insoluble drug delivery strategies: review of recent advances and business prospects. Acta Pharm. Sin. B 5, 442–453. 10.1016/j.apsb.2015.07.003. [PubMed: 26579474]

Kao C-T, Chen Y-J, Ng H-Y, Lee AK-X, Huang T-H, Lin T-F, Hsu T-T, 2018. Surface modification of calcium silicate via mussel-inspired polydopamine and effective adsorption of extracellular matrix to promote osteogenesis differentiation for bone tissue engineering. Materials 11. 10.3390/ma11091664.

Karageorgiou V, Kaplan D, 2005. Porosity of 3D biomaterial scaffolds and osteogenesis. Biomaterials 26, 5474–5491. 10.1016/j.biomaterials.2005.02.002. [PubMed: 15860204]

Kim S, Park CB, 2010. Mussel-inspired transformation of CaCO3 to bone minerals. Biomaterials 31, 6628–6634. 10.1016/j.biomaterials.2010.05.004. [PubMed: 20541803]

Ku SH, Ryu J, Hong SK, Lee H, Park CB, 2010. General functionalization route for cell adhesion on non-wetting surfaces. Biomaterials 31, 2535–2541. 10.1016/j.biomaterials.2009.12.020. [PubMed: 20061015]

Lee H, Dellatore SM, Miller WM, Messersmith PB, 2007. Mussel-Inspired surface chemistry for multifunctional coatings. Science 318, 426–430. 10.1126/science.1147241. [PubMed: 17947576]

Lee H, Rho J, Messersmith PB, 2009. Facile conjugation of biomolecules onto surfaces via mussel adhesive protein Inspired coatings. Adv. Mater. 21, 431–434. 10.1002/adma.200801222. [PubMed: 19802352]

Lee SJ, Lee D, Yoon TR, Kim HK, Jo HH, Park JS, Lee JH, Kim WD, Kwon IK, Park SA, 2016. Surface modification of 3D-printed porous scaffolds via mussel-inspired polydopamine and effective immobilization of rhBMP-2 to promote osteogenic differentiation for bone tissue engineering. Acta Biomater., Zwitterionic Materials 40, 182–191. 10.1016/j.actbio.2016.02.006.

Li D, Tang T, Lu J, Dai K, 2009. Effects of flow shear stress and mass transport on the construction of a large-scale tissue-engineered bone in a perfusion bioreactor. Tissue Eng. 15, 2773–2783. 10.1089/ten.tea.2008.0540.

Liebscher J, 2019. Chemistry of polydopamine – scope, variation, and limitation. Eur. J. Org Chem. 2019, 4976–4994. 10.1002/ejoc.201900445.

Liebscher J, Mrówczyński R, Scheidt HA, Filip C, Hădade ND, Turcu R, Bende A, Beck S, 2013. Structure of polydopamine: a never-ending story? Langmuir 29, 10539–10548. 10.1021/la4020288. [PubMed: 23875692]

Lu X, Leng Y, 2005. Theoretical analysis of calcium phosphate precipitation in simulated body fluid. Biomaterials 26, 1097–1108. 10.1016/j.biomaterials.2004.05.034. [PubMed: 15451629]

Marques CF, Perera FH, Marote A, Ferreira S, Vieira SI, Olhero S, Miranda P, Ferreira JMF, 2017. Biphasic calcium phosphate scaffolds fabricated by direct write assembly: mechanical, anti-microbial and osteoblastic properties. J. Eur. Ceram. Soc. 37, 359–368. 10.1016/j.jeurceramsoc.2016.08.018.

Morgan EF, Keaveny TM, 2001. Dependence of yield strain of human trabecular bone on anatomic site. J. Biomech. 34, 569–577. 10.1016/S0021-9290(01)00011-2. [PubMed: 11311697]

Muthusami S, Senthilkumar K, Vignesh C, Ilangovan R, Stanley J, Selvamurugan N, Srinivasan N, 2011. Effects of Cissus quadrangularis on the proliferation, differentiation and matrix mineralization of human osteoblast like SaOS-2 cells. J. Cell. Biochem. 112, 1035–1045. 10.1002/jcb.23016. [PubMed: 21308732]

Parisuthiman D, Singhatanadgit W, Dechatiwongse T, Koontongkaew S, 2009. Cissus quadrangularis extract enhances biomineralization through up-regulation of MAPK-dependent alkaline phosphatase activity in osteoblasts. In Vitro Cell. Dev. Biol. Anim. 45, 194–200. [PubMed: 19057968]

Potu BK, Rao MS, Nampurath GK, Chamallamudi MR, Prasad K, Nayak SR, Dharmavarapu PK, Kedage V, Bhat KM, 2009. Evidence-based assessment of antiosteoporotic activity of petroleum-ether extract of Cissus quadrangularis Linn. on ovariectomy-induced osteoporosis. Ups. J. Med. Sci. 114, 140–148. 10.1080/03009730902891784. [PubMed: 19736603]

Rim NG, Kim SJ, Shin YM, Jun I, Lim DW, Park JH, Shin H, 2012. Mussel-inspired surface modification of poly(l-lactide) electrospun fibers for modulation of osteogenic differentiation of human mesenchymal stem cells. Colloids Surf. B Biointerfaces 91, 189–197. 10.1016/j.colsurfb.2011.10.057. [PubMed: 22118890]

Ryu Jungki, Ku Sook Hee, Lee Haeshin, Park Chan Beum, 2010. Mussel-Inspired polydopamine coating as a universal route to hydroxyapatite crystallization. Adv. Funct. Mater. 20, 2132–2139. 10.1002/adfm.200902347.

Sarkar N, Bose S, 2019. Liposome-Encapsulated Curcumin-Loaded 3D Printed Scaffold for Bone Tissue Engineering. ACS Applied Materials & Interfaces 11 (19), 17184–17192. 10.1021/acsami.9b01218. [PubMed: 30924639]

Shirwaikar A, Khan S, Malini S, 2003. Antiosteoporotic effect of ethanol extract of Cissus quadrangularis Linn. on ovariectomized rat. J. Ethnopharmacol. 89, 245–250. 10.1016/j.jep.2003.08.004. [PubMed: 14611887]

Siddiqua A, Mittapally S, 2017. A review on Cissus quadrangularis. Pharma Innov. 6, 329.

Stohs SJ, Ray SD, 2013. A review and evaluation of the efficacy and safety of Cissus quadrangularis extracts. Phytother Res. 27, 1107–1114. 10.1002/ptr.4846. [PubMed: 22976133]

Tarafder S, Balla VK, Davies NM, Bandyopadhyay A, Bose S, 2013a. Microwave-sintered 3D printed tricalcium phosphate scaffolds for bone tissue engineering. J. Tissue Eng. Regen. Med. 7, 631–641. 10.1002/term.555. [PubMed: 22396130]

Tarafder S, Bose S, 2014. Polycaprolactone-coated 3D printed tricalcium phosphate scaffolds for bone tissue engineering: in vitro alendronate release behavior and local delivery effect on in vivo osteogenesis. ACS Appl. Mater. Interfaces 6, 9955–9965. 10.1021/am501048n. [PubMed: 24826838]

Tarafder S, Davies NM, Bandyopadhyay A, Bose S, 2013b. 3D printed tricalcium phosphate bone tissue engineering scaffolds: effect of SrO and MgO doping on in vivo osteogenesis in a rat distal femoral defect model. Biomater. Sci. 1, 1250–1259. 10.1039/C3BM60132C. [PubMed: 24729867]

Vetsch JR, Betts DC, Müller R, Hofmann S, 2017. Flow velocity-driven differentiation of human mesenchymal stromal cells in silk fibroin scaffolds: a combined experimental and computational approach. PloS One 12, e0180781. 10.1371/journal.pone.0180781. [PubMed: 28686698]

Vu AA, Bose S, 2019. Effects of vitamin D 3 release from 3D printed calcium phosphate scaffolds on osteoblast and osteoclast cell proliferation for bone tissue engineering. RSC Adv. 9 (60), 34847–34853. 10.1039/C9RA06630F.

Vu AA, Bose S, 2020. Vitamin D3 Release from Traditionally and Additively Manufactured Tricalcium Phosphate Bone Tissue Engineering Scaffolds. Ann. Biomed. Eng. 48 (3), 1025–1033. 10.1007/s10439-019-02292-3. [PubMed: 31168676]

Vu AA, Robertson SF, Ke D, Bandyopadhyay A, Bose S, 2019. Mechanical and biological properties of ZnO, SiO_2, and Ag_2O doped plasma sprayed hydroxyapatite coating for orthopaedic and dental applications. Acta Biomater. 92, 325–335. 10.1016/j.actbio.2019.05.020. [PubMed: 31082568]

Wang H, Lin C, Zhang X, Lin K, Wang X, Shen SG, 2019. Mussel-Inspired polydopamine coating: a general strategy to enhance osteogenic differentiation and osseointegration for diverse implants. ACS Appl. Mater. Interfaces 11, 7615–7625. 10.1021/acsami.8b21558. [PubMed: 30689334]

Yu W, Bien-Aime S, Mattos M, Alsadun S, Wada K, Rogado S, Fiorellini J, Graves D, Uhrich K, 2016. Sustained, localized salicylic acid delivery enhances diabetic bone regeneration via prolonged mitigation of inflammation. J. Biomed. Mater. Res. 104, 2595–2603. 10.1002/jbm.a.35781.

Zhao F, van Rietbergen B, Ito K, Hofmann S, 2018. Flow rates in perfusion bioreactors to maximise mineralisation in bone tissue engineering in vitro. J. Biomech. 79, 232–237. 10.1016/j.jbiomech.2018.08.004. [PubMed: 30149981]

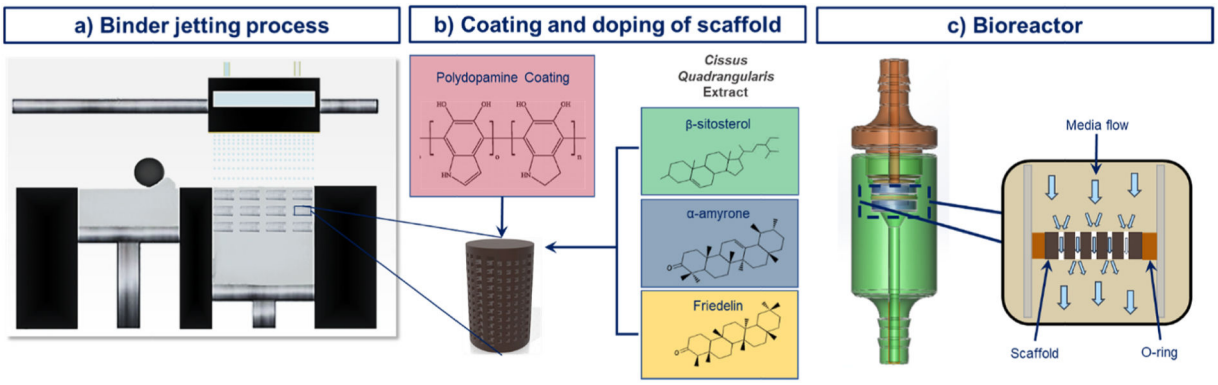

Fig. 1.

a) Additively manufactured β-TCP scaffolds, b) scaffolds coated with polydopamine and loaded with Cissus Quadrangularis extract containing ketosteroids, and c) scaffolds in perfusion flow reactor during cell culture.

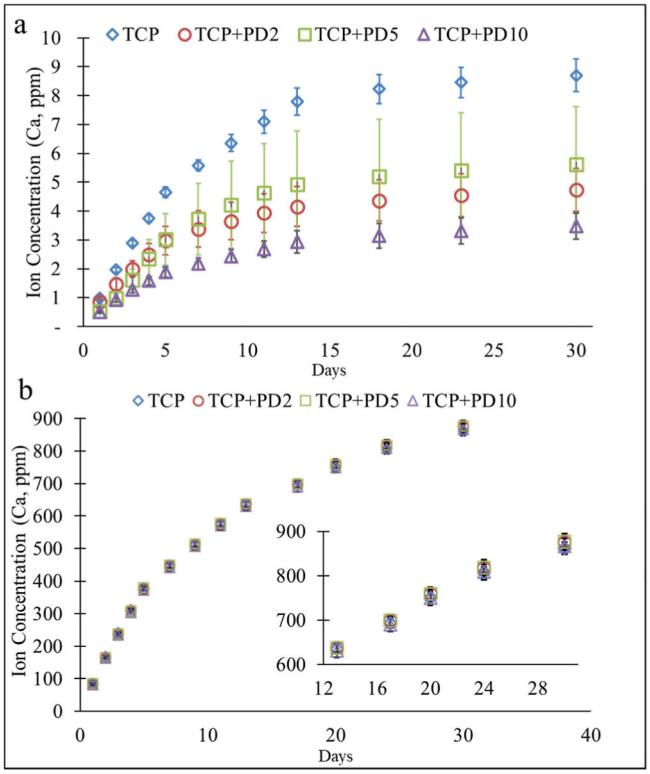

Fig. 2.

Cumulative calcium ion release plots from samples coated from starting dopamine HCL concentrations of 0, 2, 5, and 10 mg/mL. (a) Samples showed an inverse relationship between coating concentration and ion release in physiological pH 7.4, (b) in pH 5, no discernable difference in ion release was seen between compositions.

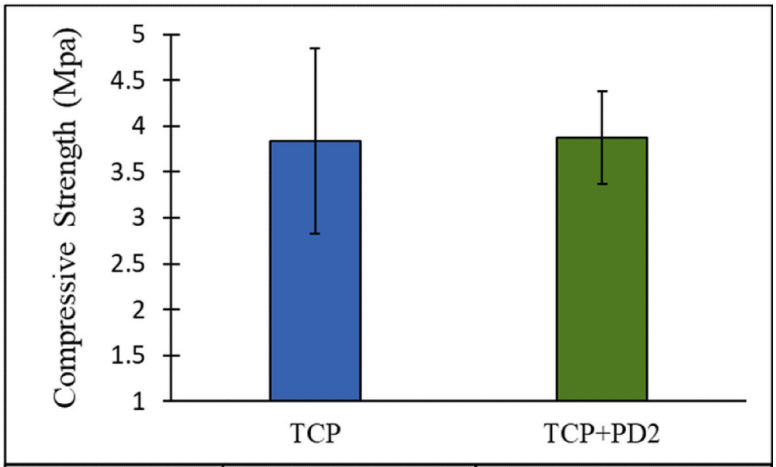

Scaffold Composition	Compressive Strength (MPa)	Young's Modulus (MPa)
TCP	3.84 ± 1.01	328 ± 60.6
TCP+PD2	3.88 ± 0.51	326 ± 43.6

Fig. 3.

Compression test results for TCP and TCP + PD2 scaffolds with 400-μm design porosity showed that the scaffolds to be used for *in vivo* maintained their strength after PD coating (n = 5).

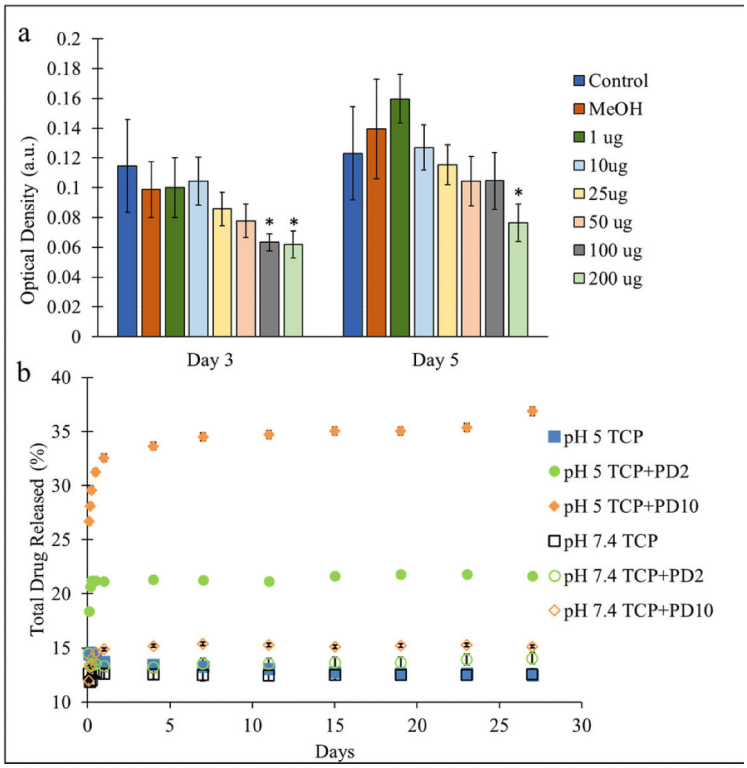

Fig. 4.

(a) Effects of CQE concentration (μg/mL) on osteoblast viability over 3 and 5 days, with concentrations between 1 and 50 μg not showing cytotoxic effects (*$p < 0.05$, $n = 6$). (b) Drug release profiles from TCP disks loaded with 1 mg of CQE in pH 5 and pH 7.4 buffers. Samples coated using higher dopamine HCl concentrations showed greater release of the drug initially and over time, especially in acidic conditions.

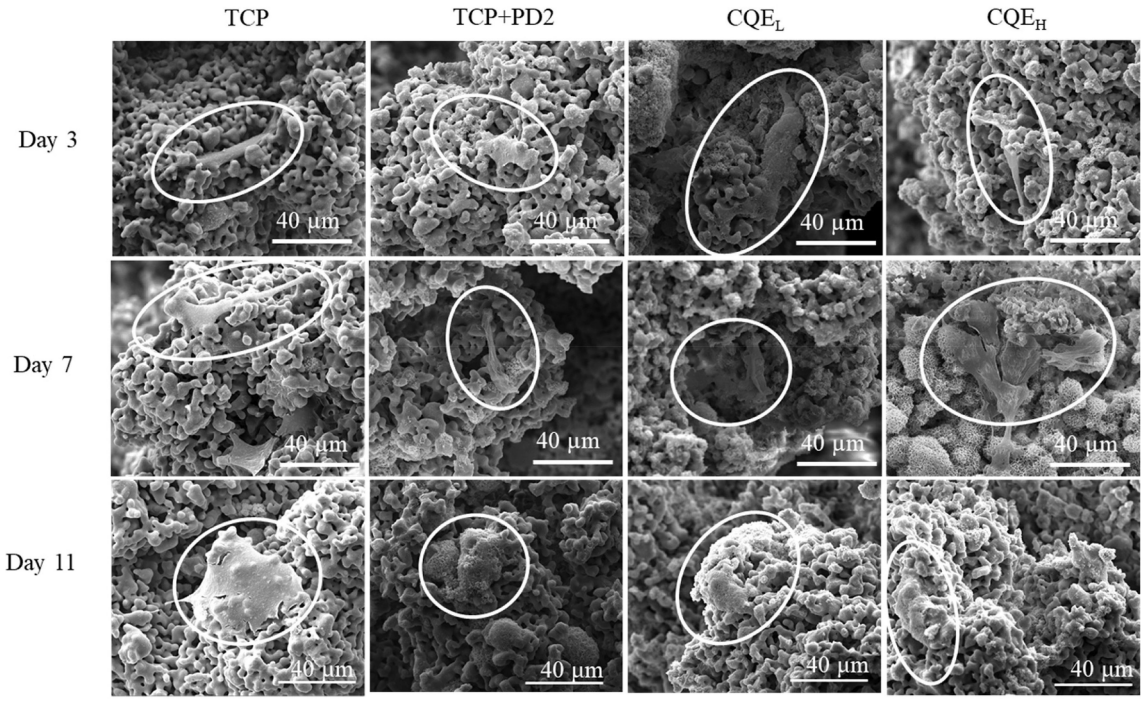

Fig. 5.

SEM images of osteoblast cells on scaffolds after 3, 7, and 11 days of static culture. Pure TCP samples showed broader cell morphologies that were less integrated into the scaffolds than PD and CQE-loaded compositions.

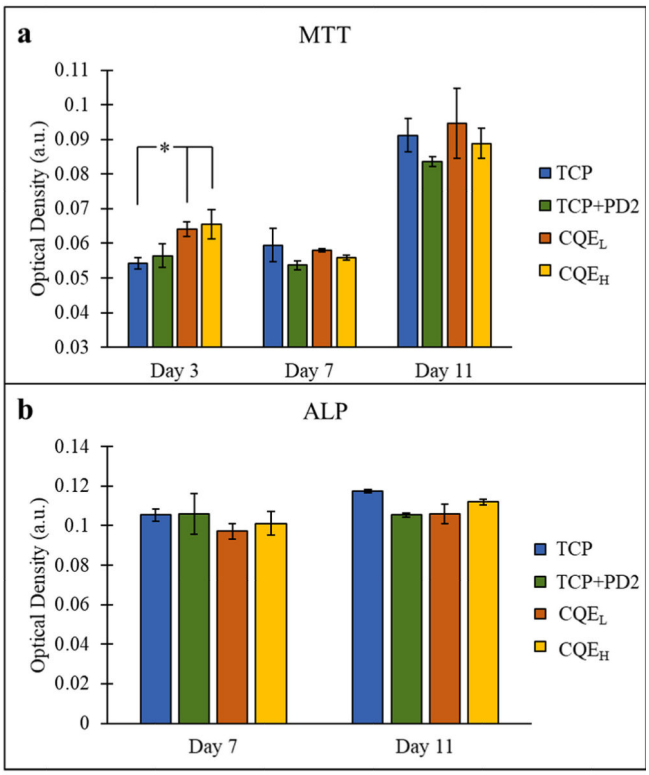

Fig. 6.

(a) MTT assay of the static culture showed a significant difference on day 3 between CQE_L and CQE_H containing 200 and 500 μg of CQE, and TCP (*$p < 0.05$, $n = 3$). (b) ALP assay showed all compositions behaved similarly.

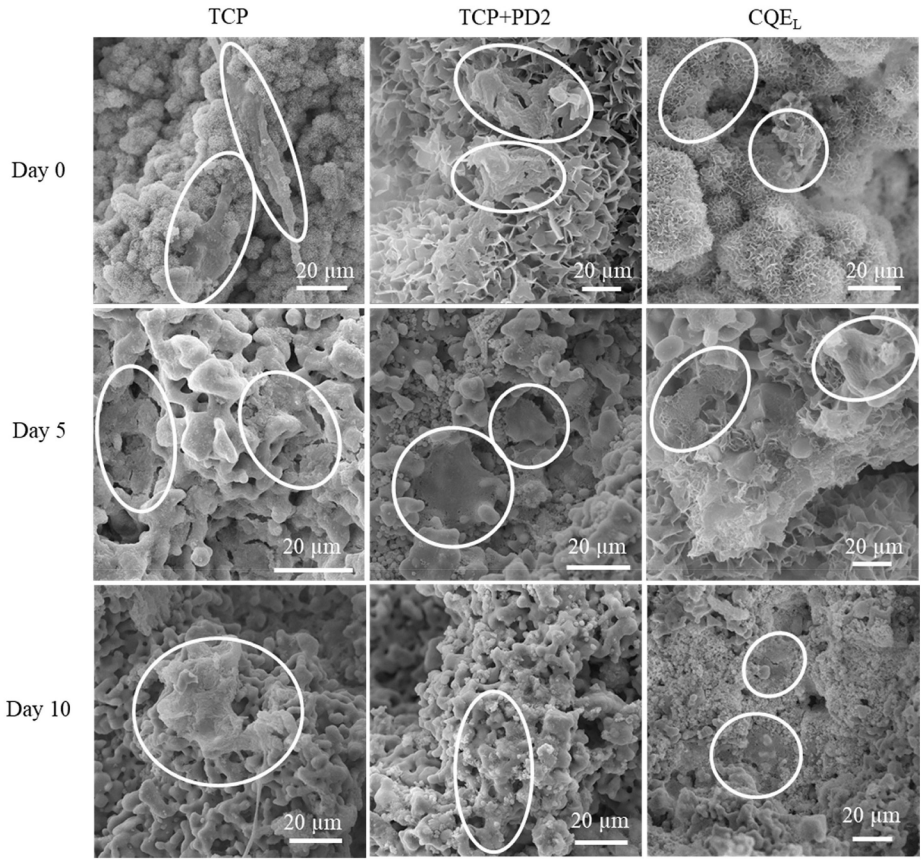

Fig. 7.

SEM images of osteoblast cells on TCP, TCP + PD2, and CQE$_L$ scaffolds after 0, 5, and 10 days of culture. Both TCP + PD2 and CQE$_L$ compositions showed greater integration and flattening of the cells to the scaffold walls.

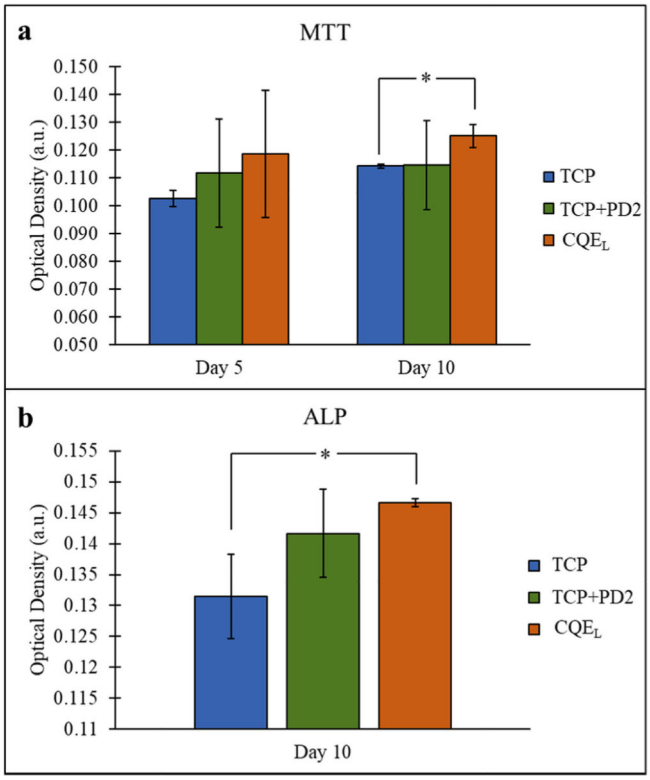

Fig. 8.

(a) MTT assay showed a significant difference on day 10 between CQE-loaded samples and control TCP, (b) ALP assay showed a significant difference on day 10 between CQE-loaded samples and control TCP. (*$p < 0.05$, $n = 3$).

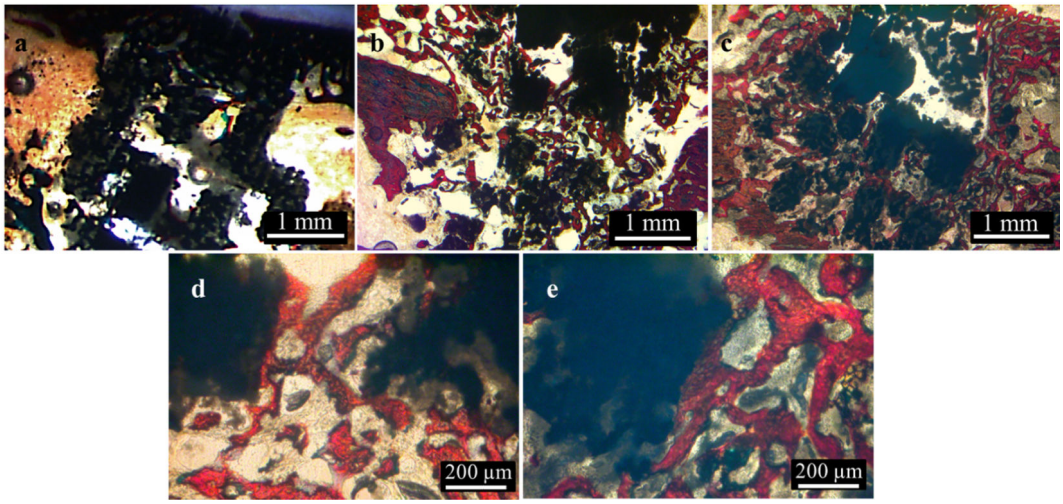

Fig. 9.

Images of histological sections with pure TCP (a), TCP + PD2 (b,d), and CQE_L (c,e) show increasing bone formation within the scaffolds with the addition of PD2 and CQE_L. Color legend: black = TCP, red = bone, brown = soft tissue/marrow. (For interpretation of the references to color in this figure legend, the reader is referred to the Web version of this article.)